Chapter 4
Lanthanide-Doped Upconversion Nanoparticles for Imaging-Guided Drug Delivery and Therapy

Zhanjun Li, Yuanwei Zhang, and Gang Han

Abstract Lanthanide-doped upconversion nanoparticles (UCNPs) possess unique anti-Stokes optical properties, in which low-energy near-infrared (NIR) excitation can be converted into high-energy UV and/or visible emission with pronounced luminescence and chemical stability. Due to the rapid development of synthesis chemistry, lanthanide-doped UCNPs can be fabricated with narrow distribution and modulated physical behaviors. These unique characters endow them unique NIR-driven imaging/delivery/therapeutic applications, especially in the cases of the deep tissue environments. Herein, we introduce both the basic concepts and the up-to-date progresses of UCNPs in material engineering, toxicology, and bio-applications in imaging, molecular delivery, and tumor therapeutics.

Keywords Upconversion nanoparticles • Optical imaging • Drug delivery • Optical therapy

4.1 Introduction

Upconversion is a nonlinear optical process in which long wavelength (usually near-infrared) photons are absorbed by upconversion materials followed by emitting photons with shorter wavelength (typically visible) [1]. Lanthanide-doped UCNPs can be excited with deep tissue-penetrating NIR light (800 nm, 925 nm, 980 nm) and emitting light in a broad range from ultraviolet (UV) to near-infrared (NIR) with various distinctive characteristics, like narrow emission band, large anti-Stokes shift, and less light scattering. These attributes make them unique optical tools for biological studies [2]. In addition, these nanoparticles are non-blinking, non-photobleaching, and extremely stable and dodged the endogenous cellular

Z. Li • Y. Zhang • G. Han (✉)
Department of Biochemistry and Molecular Pharmacology, University of Massachusetts-Medical School, 364 Plantation Street, LRB 806, Worcester, MA 01605, USA
e-mail: gang.han@umassmed.edu

Z. Dai (ed.), *Advances in Nanotheranostics I*, Springer Series in Biomaterials Science and Engineering 6, DOI 10.1007/978-3-662-48544-6_4

fluorophore spectral window [3, 4]. Thus, low autofluorescent background can be obtained, and therapeutic trackings can be conducted both in vitro and in vivo.

The working window at both NIR excitation and NIR emission (NIR-to-NIR), which are both within the biological NIR optical transmission window (700–1,000 nm), is particularly important for in vivo imaging of small animals, because it permits deep tissue penetration beyond 3 cm and less absorption and scattering of biotissues and organs [5]. The unique advantages of UCNPs make them ideal nanoplatform for diverse applications in both imaging and therapy. (1) They can serve as background-free optical probes for targeted imaging [6]. (2) They can be adapted as nanocarriers to precisely deliver therapeutic cargoes, in which way the side effects are minimized in nearby tissues and organs [7]. (3) UCNPs can be used as remote control photoswitches to precisely control the therapeutic procedures in deep tissue [8].

4.2 Engineering of UCNPs for Biomedical Applications

4.2.1 Basic Mechanism of UCNPs

In general, lanthanide-doped UCNPs contain three essential components, (1) sensitizer (usually Yb^{3+}), (2) emitter (usually Tm^{3+}, Er^{3+}, Ho^{3+}), and (3) host matrix. Because of the requirements in the matching of energy levels, the most effective sensitizer/emitter pairs are found to be Yb/Er, Yb/Tm, and Yb/Ho (Fig. 4.1). The upconversion host matrix must have low phonon energies; thus, lattice stress and nonradiative pathways can be minimized. In general, hexagonal $AReF_4$ (e.g., A: Li/Na/K, Re: Y/Lu/Gd) is broadly considered as the best host matrix for UCNPs [9–11]. Recently, we found that Nd^{3+}, which has a strong absorption at ~800 nm, can be used as a novel sensitizer (Fig. 4.2) [12]. By the fabrication of a tri-doped $NaYF_4$:Nd,Yb,Er/Tm, the excitation wavelength of lanthanide-based UCNPs can be transferred to 800 nm. This design not only offers a new excitation choice but also can decrease the thermal effect obviously because the absorption coefficient of

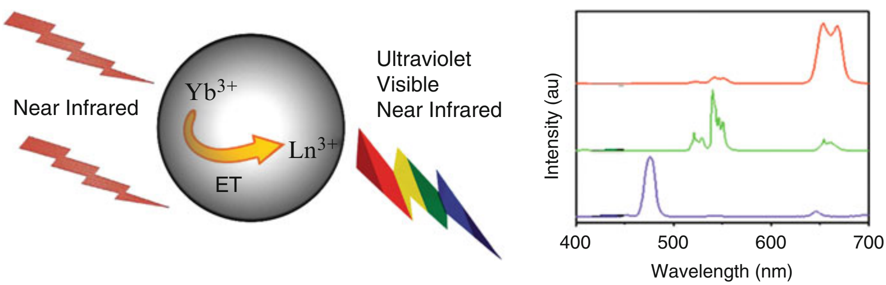

Fig. 4.1 Schematic representation of the excitation/emission and interatomic energy transfer profiles of UCNPs and examples of upconversion emission spectra upon 980 nm excitation

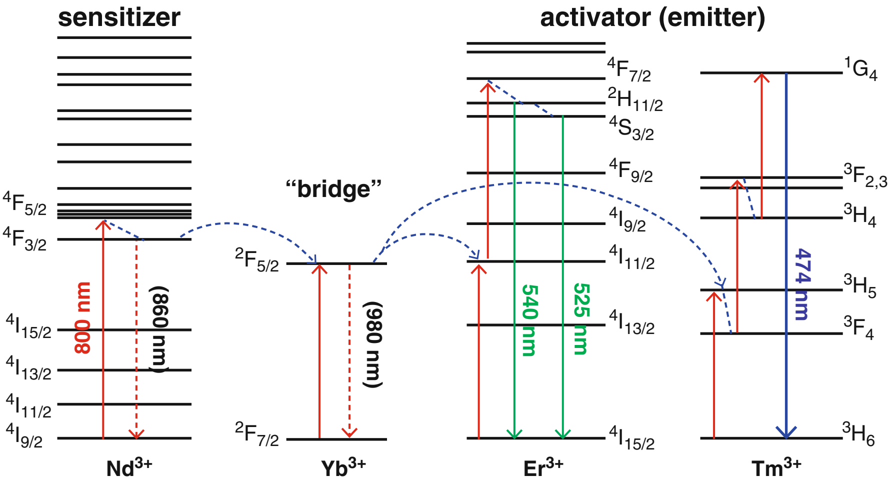

Fig. 4.2 Upconversion process of Nd/Yb/Er(Tm) tri-dopants system with 800 nm excitation (Reproduced from Ref. [12] by permission of John Wiley & Sons Ltd.)

water at 800 nm is several magnitudes lower than that at 980 nm. Thus, we can minimize the thermal side effect during upconversion imaging or therapy by using these tri-doped UCNPs. It should be noted that the upconversion efficiency of these simple tri-doped system is low because of the reverse energy transfer from Er/Tm to Nd. Soon after our report, this problem was solved by fabrication of a core@shell structure which will be discussed later.

4.2.2 Synthesis of UCNPs

Due to the requirement of narrow size distribution and high dispersibility for biological studies, thermal decomposition and solvothermal synthesis techniques are the most widely employed strategies. In addition, with nicely controlled conditions, like temperature, materials ratio, and selected component, the UCNPs can be fabricated with diverse sizes and shapes [13]. In order to generate solvent dispersible UCNPs, Yan et al. developed a high-temperature decomposition strategy, and a variety of monodispersed cubic and hexagonal $NaYF_4$-based nanocrystals were fabricated with high quality [14]. Generally, the size and morphology of UCNPs can be well controlled by decomposing metal trifluoroacetate precursors at high temperature in mixed solvents of oleic acid, oleicamine, and octadecene. This strategy has become a most typical method to fabricate UCNPs, and the critical synthesis parameters have been thoroughly investigated, such as coordinating solvent compositions [15], decomposition temperature [16], starting material species and ratio [17], and core/shell structures [18]. For example, to synthesize high luminescent and ultrasmall upconversion nanoparticles with biomolecules of comparable size, Chow et al. fabricated ca. 11 nm -$NaYF_4$:Yb,Er and -$NaYF_4$:Yb,Tm UCNPs in pure oleylamine solutions, and further upconversion efficiency was improved by coating inert shell structure [15].

Using hydrothermal synthesis strategy, UCNPs with uniform sizes and shapes can also be achieved. Generally, UCNPs are obtained by mixing fluoride salts (e.g., NH_4F) with lanthanide compounds in solvent with high boiling point such as ethylene glycol and reacted under high temperature and pressure. For example, using this method, β-phased $NaYF_4$ UCNPs were fabricated with corresponding oleate precursor [19]. More sophisticated strategy was developed using a liquid-solid-solution phase-transfer method in water/alcohol/oleic acid mixture to fulfill predictable size, shapes, and phase UCNPs [20, 21].

4.2.3 UCNPs with Core@shell Structures

As optical bio-probes, high fluorescent efficiency will be required in water solutions. However, the OH and NH_2 groups surrounding the surface of UCNPs could quench the excited states through nonradiative relaxation processes. Nevertheless, when the nanoparticle sizes go smaller, those quenching effects become more severe. In order to conquer this problem, an inert shell (undoped $NaYF_4$, $NaGaF_4$, $NaLuF_4$, etc.) is usually needed to protect the upconverting active core (namely, a core@shell nanostructure) from the outside quenching reagents. Thus, the possibility of energy loss from the active core is highly reduced and consequently enhancing upconversion efficiency. For example, Kong and Zhang carefully studies β-$NaYF_4$:Yb^{3+},Er^{3+}@β-$NaYF_4$ core-shell structure; from the kinetics analysis, they discovered the quenching effect of luminescent centers can be effectively reduced by homogeneous coating with $NaYF_4$ shell and conduct luminescence enhancing [22]. Later on, Liu et al. showed direct evidence for the surface quenching effect related to the nanoparticle sizes in $NaGaF_4$:Yb,Tm. They also intensified the optical integrity, and surface quenching effects of the nanoparticles can be greatly preserved after an inert thin shell coating ($NaGdF_4$:Yb,Tm@$NaGdF_4$) (Fig. 4.3) [23].

Usually, β-NaY/Gd/LuF_4 is considered to be the best upconversion matrix. And the same host matrix will be used in the active core@inert shell design. Quite interestingly, we find that an epitaxial CaF_2 heteroshell can increase the upconversion efficiency of α-$NaYF_4$ for hundreds of times (Fig. 4.4). The UV upconversion in α-$NaYbF_4$:Tm@CaF_2 (362 nm) is even higher than β-$NaYF_4$:30 %Yb, 0.5 %Tm@β-NaYF4 and larger β-phase counterparts [24]. In addition, the CaF_2 coating is found to be more effective in resisting quenching in aqueous medium to preserve the upconverting UV emissions. In the same material, we also find that CaF_2 heteroshell could increase the NIR emission of α-$NaYbF_4$:0.5 %Tm for 35 times with a relative high NIR-to-NIR quantum yield of 0.6 % under low-energy excitation of 0.3 W/cm^2 [5].

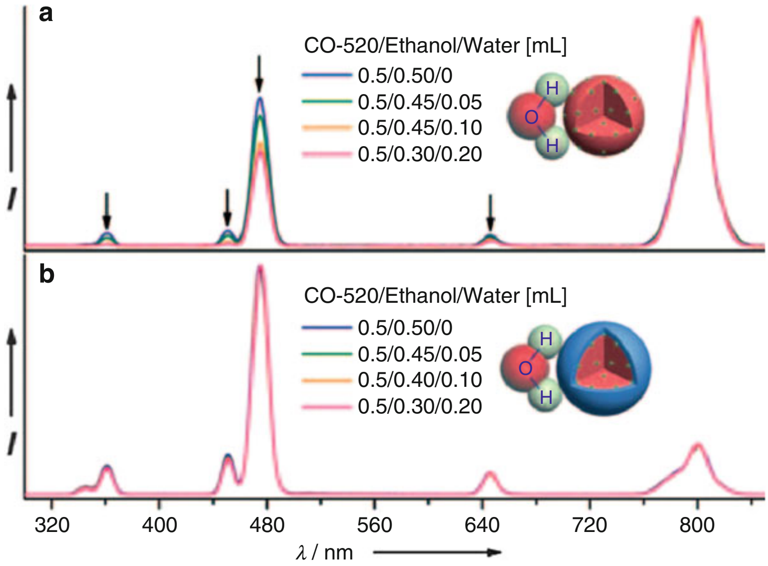

Fig. 4.3 Upconversion emission spectra of (**a**) $NaGdF_4$:25 %Yb/0.3 %Tm (15 nm) and (**b**) corresponding core/shell nanoparticles (20 nm) in nonylphenylether/ethanol/water solutions with different water ratio (Reproduced from Ref. [23] by permission of John Wiley & Sons Ltd.)

For the Nd^{3+}-sensitized UCNPs, the upconversion efficiency using 800 nm excitation is relatively low than the traditional 980 nm-excited counterparts. In order to address this issue, Zhao and Yao fabricated quenching-shielded sandwich-structured rare-earth nanoparticles that have high upconversion emissions with excitation at wavelength of 800 nm, as shown in Fig. 4.5 [25]. In this system, the nanostructure has been well defined to eliminate the potential cross-relaxation pathways between the activator and sensitizer by introducing an interlayer of $NaYF_4$:Yb^{3+}. The emission intensity of the nanoparticles reached maximum when the interlayer thickness was ~1.45 nm ($NaYF_4$:Yb^{3+}). This well-defined unique nanostructure is essential to eliminate the deleterious cross-relaxation pathways between the activator and sensitizer by means of a precisely controlled transition layer. The as-synthesized UCNPs are even brighter than conventional 980 nm-excited nanoparticles at low excitation power density of 0.5 W/cm^2. Further, the use of 800 nm laser source instead of 980 nm one is able to increase the penetration depth in biotissue and suppress overheating.

By simultaneously harnessing the sensitizer Yb^{3+} and Nd^{3+} together into different shell layers of one single nanoparticle, Feng Wang et al. designed a kind of core@multishell nanostructure named $NaGdF_4$:Yb,Tm @$NaGdF_4$ @$NaYbF_4$:Nd @ $Na(Yb,Gd)F_4$:Ho @$NaGdF_4$, in which different emission can be realized by altering excitation light source (976 nm/blue, 808 nm/green, Fig. 4.6) [26]. Under 976 nm laser excitation, the excitation light will be absorbed by Yb^{3+} in both the core and the shell of the UCNPs. But the energy back transfer from Ho^{3+} to Nd^{3+} will inhibit

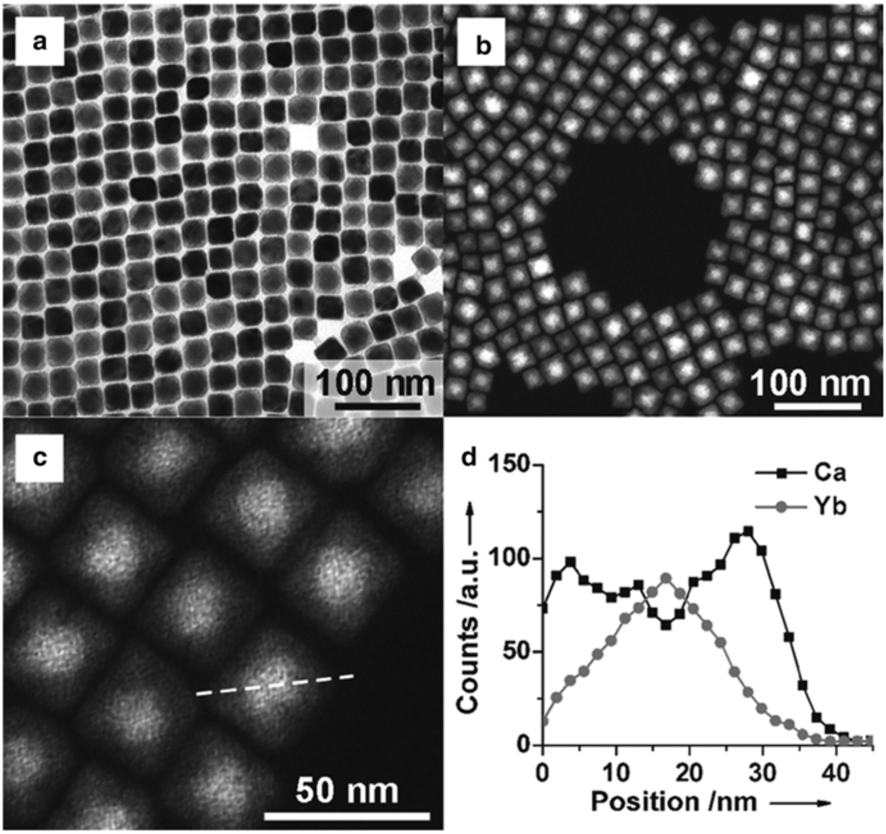

Fig. 4.4 Heteroshell structure of α-$NaYbF_4$:Tm@CaF_2. (**a**) TEM, (**b**) high-angle annular dark-field STEM, (**c**) linear EDX scanning of a single UCNP, and (**d**) corresponding elemental ratio analysis (Reproduced from Ref. [24] by permission of John Wiley & Sons Ltd.)

the emission of Ho^{3+} (green). The general emission color will be dominated by transition from Yb to Tm in the core. But, under 808 nm excitation, Nd^{3+} will be sensitized and then transfer the absorbed energy to Ho^{3+} to generate green emission. The energy transfer to the inner core is blocked by the inert $NaGdF_4$ layer between the Tm^{3+} activated core and the Ho activated shell. Thus, the 808 nm-excited emission will be dominated by Ho^{3+} (green). This kind of excitation-regulated upconversion emission properties will have great potential in the field of multichannel photoactive processes.

Lee's group synthesized a similar dual-channel upconversion system, and more importantly, they demonstrated the two-way photoswitching applications of this novel UCNPs (Fig. 4.7) [27]. The photoisomerization between spiropyran and merocyanine can be regulated by UV and visible light. The maximum absorption peaks of spiropyran and merocyanine that locate at 342 nm and 560 nm overlap well with the UV emission from the Tm^{3+} and Er^{3+}, respectively. Thus, under excitation

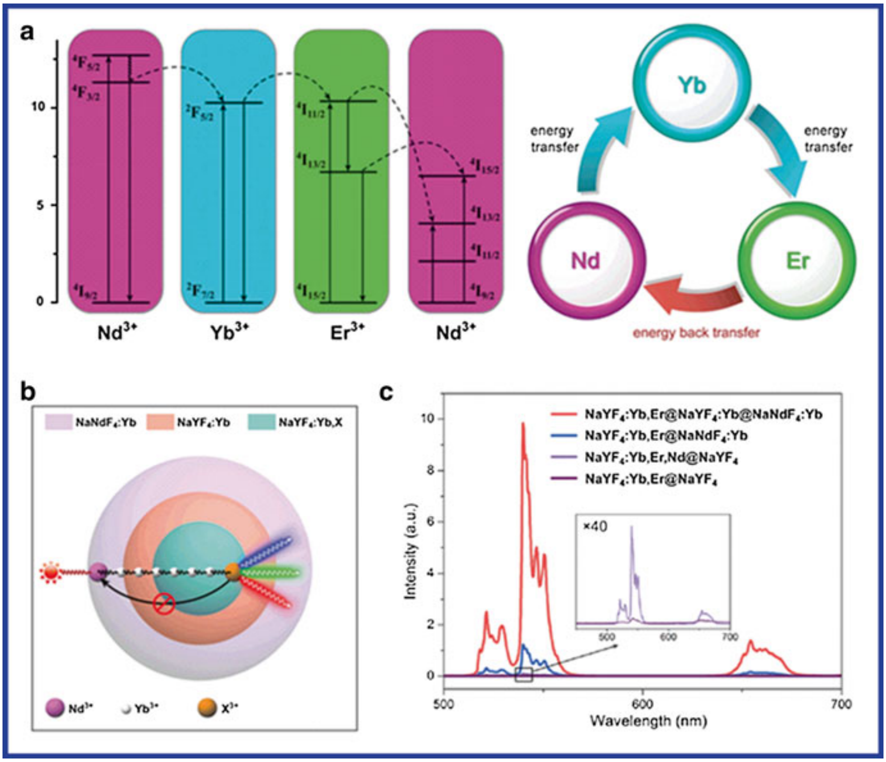

Fig. 4.5 Bright upconversion under 800 nm excitation by engineering core@shell@shell structure. (**a**) Simplified energy-level diagrams depicting the energy transfer between Nd, Yb, and Er ions upon 800 nm excitation. (**b**) Schematic illustration of the proposed energy transfer mechanisms in the quenching-shield sandwich-structured UCNPs; **c** upconversion emission spectra of the as-synthesized UCNPs (Reproduced from Ref. [25] by permission of John Wiley & Sons Ltd.)

of 808 nm, UV emission will be activated by energy transfer from Nd^{3+} to Tm^{3+}, leading to the photoisomerization of spiropyran to merocyanine (pink solution). Thereafter, under the excitation of 980 nm laser, green emission from Er^{3+} can be generated, leading to the photoisomerization of merocyanine back to spiropyran (colorless).

4.2.4 *Surface Modification for Upconversion Enhancing and Bio-conjugation*

Post-modification of the surface of UCNPs by charged or polar groups can offer them aqueous solubilities and biocompatibilities. In this regard, several strategies have been developed to transfer the as-synthesized hydrophobic nanoparticles into

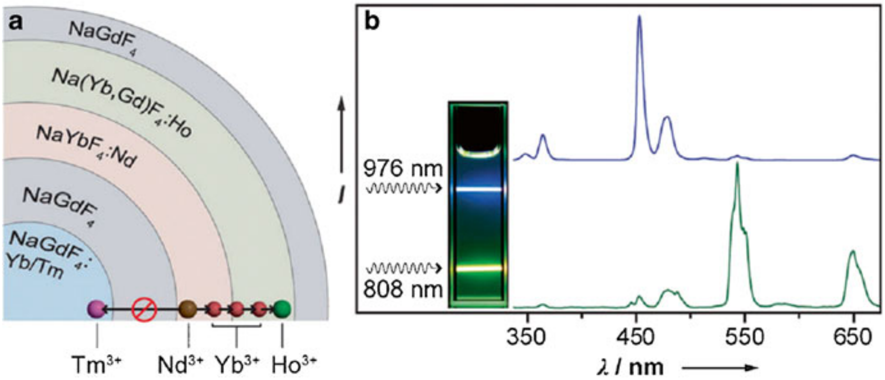

Fig. 4.6 (**a**) Schematic design of tuning the Nd-sensitized upconversion process through nanostructural engineering. (**b**) Emission spectra of the multishelled nanoparticles under excitation at 808 and 976 nm, respectively. Inset: digital camera photograph of corresponding solution sample (Reproduced from Ref. [26] by permission of John Wiley & Sons Ltd.)

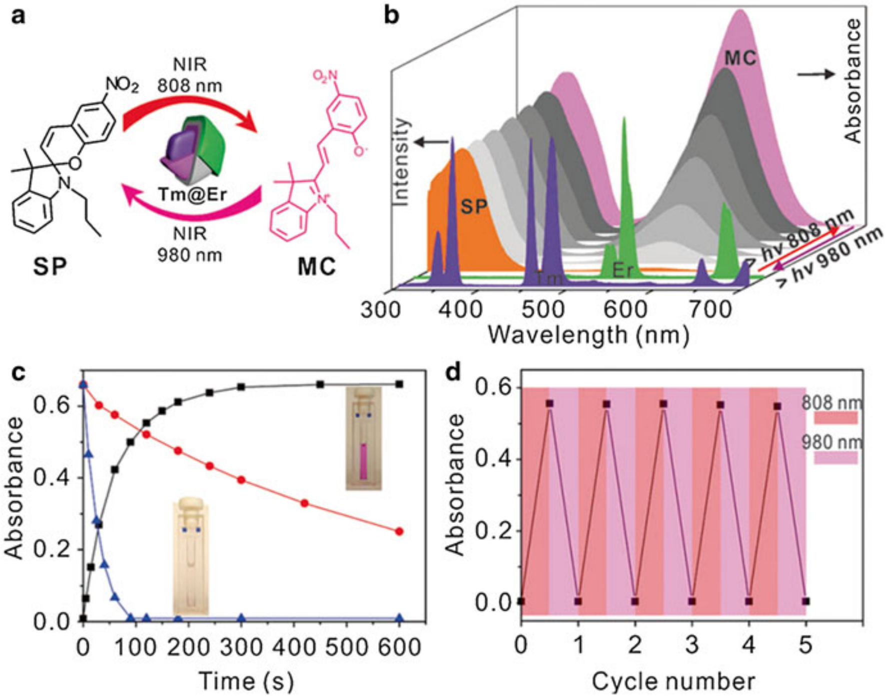

Fig. 4.7 (**a**) Illustration of two-way photoswitching of spiropyran by using UCNPs with dual NIR excitations. (**b**) Tm^{3+} and Er^{3+} emissions from the UCNPs under 808 nm and 980 nm excitations and the evolution of the UV/vis absorption spectrum of the photoisomerization. (**c**) Kinetic monitoring of the photoswitching reaction. The red dotted line shows the kinetics of the reaction of merocyanine to spiropyran. (**d**) Dual NIR-driven photoswitching of spiropyran over many cycles in THF/methanol (9/1, v/v) solution by monitoring the absorbance of merocyanine at 560 nm (Reproduced from Ref. [27] by permission of John Wiley & Sons Ltd)

water solution using amphiphilic polymer [28] and ligand oxidation [29]. Firstly, Yadong Li's group developed a polyol solvent ligand exchange method to transfer hydrophobic inorganic nanocrystals from organic solvent to aqueous solution by modifying polyelectrolytes, such as poly(acrylic acid), poly(allylamine), and poly(sodium styrenesulfonate) [30]. In this method, a toluene solution containing hydrophobic nanocrystals is rapidly injected into a heated mixture of polyol (diethylene glycol) and exchanging ligands. The solution becomes turbid immediately because of the insolubility of hydrophobic nanocrystals in the polar solvent. Upon continued heating at a higher temperature close to the boiling point of the solvent, the solution slowly turns clear, indicating the occurrence of ligand exchange and dissolution of nanocrystals in DEG. The nanocrystals can then be precipitated, for example, by adding excess amount of diluted aqueous solution of hydrochloric acid and finally redispersed in water by transforming remaining uncoordinated groups into ionized form. This method is found also effective in the case of UCNPs.

Another effective phase transition method was developed by Angang Dong et al., characterized by using $NOBF_4$ (Fig. 4.8) [31]. In this method, nitrosonium tetrafluoroborate ($NOBF_4$) is used to replace the original organic ligands attached to the nanoparticle surface, stabilizing the nanoparticles in various polar, hydrophilic media such as N,N-dimethylformamide for years of storage. The hydrophilic nanoparticles obtained can subsequently be further functionalized by using a variety of capping reagents. Furthermore, the phase transition and ligand exchange reaction is so fast that it can be finished in several minutes. And more significantly, the hydrophilic nanoparticles obtained by $NOBF_4$ treatment can readily undergo secondary surface modification due to the weak binding affinity of BF_4^- anions to the particle surface, allowing reversible phase transition.

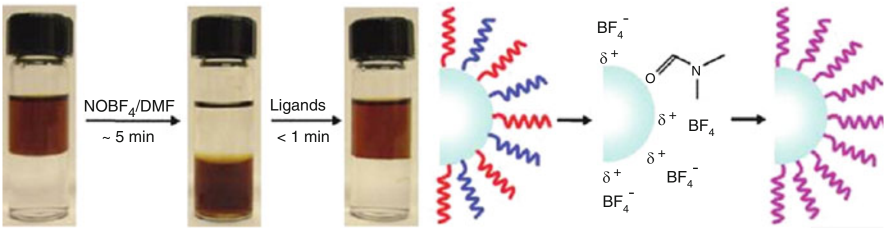

Fig. 4.8 Scheme of the phase transition and ligand exchange procedure by using $NOBF_4$ (Reprinted with the permission from Ref. [31]. Copyright 2011 American Chemical Society)

4.3 Biosafety of UCNPs

4.3.1 Internalization of UCNPs into Cells

The toxic effects of UCNPs in cells and animals are determined by the cell internalization and their distribution sites. Thus, the study of the internalization and distribution sites of UCNPs in cells is important in the assessment of their biosafety. Different from small molecules, it is difficult for UCNPs to cross the plasma membrane on their own. Generally, UCNPs are internalized from endocytosis process of cells. According to previous researches [32], the internalization of nanoparticles is usually regulated through a process termed pinocytosis which involves at least four basic mechanisms: (1) micropinocytosis (>1 μm), (2) clathrin-mediated endocytosis (~120 nm), (3) caveolae-mediated endocytosis (~60 nm), and (4) clathrin- and caveolae-independent endocytosis. The real mechanism might vary depending on many factors, such as particle sizes, surface ligands, and incubation conditions. The most common interactions are electrostatic interactions between the UCNPs and the plasma membrane of UCNPs (negatively charged). According to current report, the surface charge of UCNPs severely affects their cellular uptake efficiency. Generally, positive charge can greatly enhance cellular uptake of UCNPs, which is significantly higher than their neutral and negative counterparts. For example, Wong et al. [33] found that positively charged UCNPs modified with polyetherimide (PEI) (50 nm, 51 mV) had five times of cellular uptake than that of neutral UCNPs modified with polyvinylpyrrolidone (PVP). And negatively charged UCNPs modified with poly(acrylic acid) (PAA) (50 nm, −23 mV) showed the lowest cellular uptake efficiency. Although positive charges can facilitate the internalization of UCNPs, several studies also reported the uptake of negatively charged nanoparticles into cells. For example, Li's group found that citrate-modified UCNPs (20 nm, −18 mV) could be internalized by KB cells after 1 h incubation [34]. Similar results were also found in sodium glutamate and diethylene triamine pentaacetic acid-modified UCNPs [35]. In addition, it should be noted that the absorption of serum protein in vitro or in vivo might change the hydrodynamic size and surface charges significantly. On the other hand, there is still no detailed investigation on the internalization process and the intracellular distribution sites of UCNPs.

4.3.2 Biodistributions of Injected UCNPs in Mice Models

The in vivo imaging study usually applies mice model via intravenous (i.v.) injection. Except for some ultrasmall nanoparticles, the final deposition site was mainly the liver and spleen, which is usually attributed to the capture by the reticuloendothelial system (RES). To increase the systemic circulation time of injected UCNPs, a well-designed surface modification will be needed to avoid the capture by the RES. In this regard, polyethylene glycol (PEG) is usually the most effective surface ligand, and it is approved by the US Food and Drug Administration because of its low immunogenicity and antigenicity. The highly flexible chains of PEG can provide a "conformational cloud" around the particles, which prevents the surface absorption of blood components and the subsequent recognition of the RES. Li's group found that the half-life circulation time of PEG-UCNPs was about ten times (4.3 h vs. 0.4 h) as high as nude UCNPs [36]. Targeting moieties are required to increase the concentration of UCNPs in specific sites of diseases, namely, targeted delivery/imaging. In this regard, folic acid was frequently applied to modify UCNPs to fabricate targeted imaging nanoprobes, on the basis of the high affinity of folic acid and its receptor (usually highly expressed in tumor) [37]. To date, there is a series of targeting moieties developed to decrease the nonspecific distributions of UCNPs, such as tripeptide [38], chlorotoxin [39], heparin [40], and antibodies [41].

4.3.3 Excretion of UCNPs

The FDA requires that injected agents, especially the diagnosis agents, should be completely cleared in a reasonable time period. It is known that most injected agents can be excreted from the hepatobiliary or renal route. Hepatocytes serve as an important site for the elimination of injected nanoparticles through phagocytosis. In a previous report by Li's group [42], PAA-modified UCNPs could be found in the intestinal tract after 7 days postinjection, indicating the clearance via hepatobiliary transport. After 21 days postinjection, the UCNPs could only be detected in the intestinal tract and remained unchanged up to 90 days. After 115 days, almost no UCNPs could be found in the mouse. These results indicated that the internalized UCNPs can be excreted out of the body, although for a long time. Moreover, no significant change could be observed in size, size distribution, and morphology using transmission electron microscopy in the excreted UCNPs comparing with the initial nanoparticles before injection.

Renal excretion is the other vital important way for the clearance of nanoparticles. It is generally accepted that the size of nanoparticle is one of the most important determinants of the excretion pathway. Although the smallest nanostructural dimensions are *ca.* 43 nm in the glomerular capillary wall, the functional or physiologic pore size is considered to be only 4.5–5 nm in diameter, considering the combined effects of several layers of glomerular capillary [43]. Li's group studied the in vivo metabolism of sub-10 nm PEG-UCNPs labeled by radioactive ^{153}Sm, which could be observed in the bladder from 0.5 to 6 h at a concentration of 5.28 ± 0.2 %ID g^{-1} [36]. It should be noted that the particle size is the precondition of renal excretion but not the only one. $Gd_2O_3@SiO_2$ nanoparticles without PEG modification with 3.3 nm hydrodynamic diameter were found not to be excreted from the body, but deposited in the liver and lung. Only the PEG-modified ones could be found in the bladder 1 h after *i.v.* injection, indicating fast elimination by renal excretion [44]. Regarding the time that is needed for the excretion, generally, smaller particles excrete from the kidney faster, from hours to days, while bigger particles take longer time from weeks to months or even years. Gao et al. found that it needed 1.4 days for PEG-coated UCNPs (~5 nm) to be half excreted. Yet, most of the bigger counterparts (~19 nm) needed 7 days to be half excreted [45].

4.3.4 Cellular and In Vivo Toxicity of UCNPs

Quite a lot of studies have been performed to investigate the potential toxicity of UCNPs in cells. Mitochondrial metabolic activity has been generally taken to evaluate the influence of UCNPs on cell viability of normal or tumor cells. The most adopted method is the well-known MTT method. To date, many studies have been conducted with concentrations up to tens of 20 mg/mL and incubation time up to hundreds of hours and the particle sizes ranging from several nanometers to hundreds of nanometers. Nearly all the results reported more than 75 % of cell viability, indicating the weak toxic effects of UCNPs on cellular level in vitro, which is usually considered one of the advantages of UCNPs comparing with other luminescent nanoparticles such as quantum dots. On the other hand, some of the researches were also done on the influence of UCNPs on cell behavior. Han's group studied the influence of UCNPs (α-$NaYbF_4$:0.5 %Tm@CaF_2) on the proliferation and differentiation of mesenchymal stem cells. They found that PEI covalently conjugated UCNPs had no short-term influence on the cell proliferation ability. The labeled stem cells were able to undergo osteogenic and adipogenic differentiation under in vitro induction. However, the osteogenesis of the labeled stem cells seemed to have less potency comparing with the unlabeled cells [28].

For in vivo toxicology studies, related reports are relatively rare comparing with the cytotoxicity studies. However, till now, the available published data have indicated the safety of UCNPs at the dosage used for imaging and drug delivery. Zhang et al. reported that mice treated with a dose of 10 mg/kg body weight of silica-coated $NaYF_4$:Yb,Er (~30 nm) did not show any significant difference in body weight with the control group. And the health status and behavior of all the mice were observed normal through the entire experiment. Moreover, all organ weights were consistent among all the mice at all the time points ranging from 10 min to 7 days [46]. In a longer time range up to 115 days, Li's group systematically studied the long-term toxicity of PAA-coated UCNPs after *i.v.* injection. No abnormal indicators, including eating and drinking behavior, fur color, exploratory behavior, activity, and neurological status, were observed except a weak weight difference compared with the control group [42]. Although there were no reports of abnormal behavior and death after *i.v.* injection, the current evidence is still far from enough to draw the conclusion that the UCNPs are safe for biology and medicine.

4.4 UCNPs as Imaging Contrast Reagents

The upconversion property of UCNPs makes them very appealing for bio-imaging studies due to their dark background for autofluorescence derived from biological samples. The near-infrared excitation wavelength also permits deep tissue penetrations. In addition to the non-blinking and stable properties, UCNPs can conduct improved detection limits with large signal-to-noise ratio compared with classical imaging probes, like organic dyes and quantum dots. For example, β-$NaYF_4$:Er,Yb nanocrystals were fabricated for luminescence imaging studies, and the nanoparticles with size around 30 nm were found to have improved signal-to-noise ratio and to be non-photobleaching and non-blinking (Fig. 4.9) [3]. After encapsulating with amphiphilic polymer, the UCNPs can be dispersed in water solutions and further incubated with murine fibroblasts and inoculated by endocytosis. In another example, $NaYbF_4$-based UCNPs have been synthesized with CaF_2 shell coating. Both in vitro and in vivo imaging were performed with high contrast imaging properties after tail vein injection to mouse, demonstrating the efficiency for practical imaging researches [5] (Fig. 4.10).

Because many tumor cells overexpress corresponding transmembrane receptors, UCNPs with small peptide labeling are particularly interesting for tumor-targeting drug delivery tracking within complex biological systems. For example, peptide motif of c(RGD) with high binding affinity to $\alpha_v\beta_3$ integrin receptor was used to functionalize UCNPs for ex vivo and in vivo imaging studies. Intense luminescence from the tumor could be observed 24 h after injection, while the luminescence from liver was reduced significantly (Fig. 4.11). Also, due to the specific peptide labeling, the afforded nano-system was found to have more affinity to U87MG tumor cell line compared with MCF-7 tumor, suggesting the potential application as cancer detection technique [38]. Another peptide, polypeptide neurotoxins, was shown to effectively bind with many types of cancer cells of high specificity and affinity. For instance, a typical neurotoxin peptide of recombinant chlorotoxin was used to conjugate with hexagonal-phase $NaYF_4$:Yb,Er/Ce nanoparticles, which were later injected into Balb/c nude mice [39]. The sensitivity and specificity of neurotoxin-mediated UCNPs tumor targeting was readily imaged using 980 nm excitation.

UCNPs with folic acid modification were also developed for tumor-targeting studies. In one case, folic acid-coupled $NaYF_4$:Yb,Er UCNPs were fabricated and exhibit effectiveness in targeting folate-receptor overexpressing HeLa cells in vitro and HeLa tumors in vivo [37]. Therein, $NaYF_4$:Yb,Er nanocrystals were fabricated by a modified hydrothermal microemulsion strategy using 6-aminohexanoic acid. The outside amine functional group of the resulting UCNPs not only conferred excellent water solubilities but also enabled further modification by carboxylic acid-activated folic acid. After the folic acid-modified UCNPs were injected into HeLa tumor-bearing nude mice for 24 h, an upconverting luminescence signal (around 650 nm) was observed in the tumor regions, while no significant luminescence signal was detected for controlled mice injected with UCNPs without FA modification.

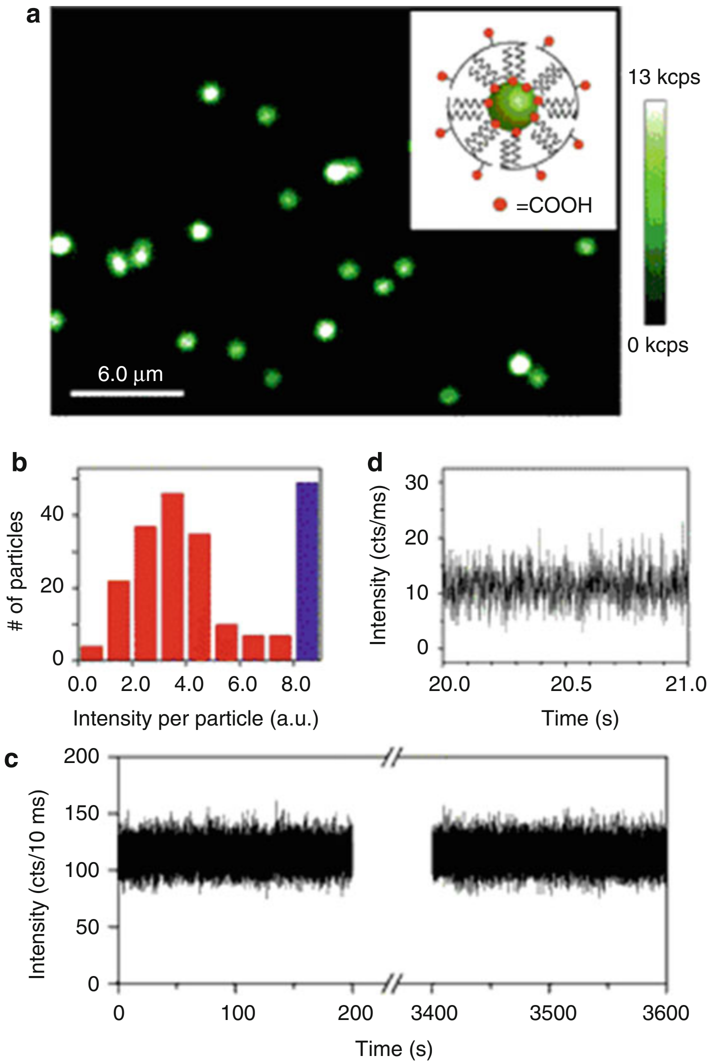

Fig. 4.9 Upconverted luminescence of individual water-soluble UCNPs. (**a**) Confocal upconverted luminescent image of individual amphiphilic polymer-coated UCNPs (schematically shown in the *inset*) sparsely dispersed on a clean cover glass. The laser power is approximately 10 mW, equivalent to approximately 5×10^6 W/cm^2. Some of the bright luminescent spots represent multiple UCNPs within the diffraction-limited area, generating saturated "white" spots in the image. (**b**) A histogram of integrated emission intensity from over 200 upconverted luminescent spots, suggesting that most of the luminescent spots are from single polymer-coated UCNPs. The data were analyzed from confocal upconverted luminescent images over a 75×75 μm area, and the number of saturated "white" spots was shown in the histogram as a *blue bar*. Such single water-soluble UCNPs also exhibit exceptional photostability (**c**) and non-blinking behavior (**d**) (Reprinted with permission from Ref. [3]. Copyright 2009 Highwire press PNAS)

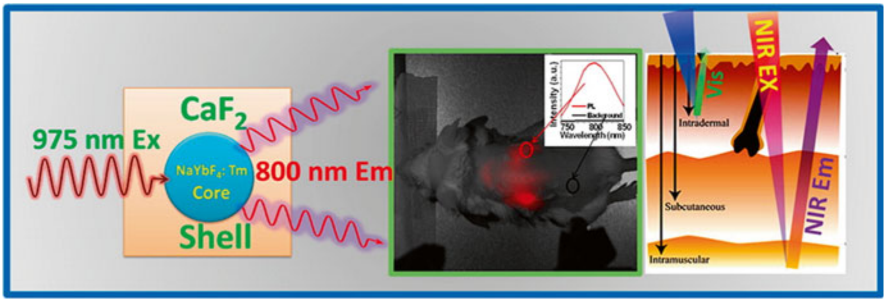

Fig. 4.10 Example of lanthanide-doped UCNPs of core/shell structures with NIR-to-NIR optical transitions and their application for small animal imaging studies plus illustration showing the better penetration of NIR light in contrast with visible light (Reprinted with the permission from Ref. [5]. Copyright 2012 American Chemical Society)

4.5 UCNPs as Drug Delivery Nanoplatform

4.5.1 UCNPs as Traditional Drug Delivery Tools

Using drug delivery carriers can greatly enhance the efficacy of pharmaceutical payloads for the improved solubility, stability, and pharmacokinetics of drugs. A wide variety of materials have been used as drug carriers, and more recently, fluorescent quantum dots have been used as platforms of optical imaging-guided carriers in real time in live organisms. However, the high toxic components in quantum dots limited its further applications for studies in cells and small animals. UCNP systems with unique optical and biocompatible components have emerged as promising candidates for traceable drug delivery.

Two of the most important UCNP-based drug delivery systems are hydrophobic pockets and porous silica shell. In the first method, drugs are encapsulated into "hydrophobic pockets" on the surface of UCNPs through hydrophobic interactions (Fig. 4.12) [47]. For example, by functionalizing the nanoparticle surface with polyethylene glycol-grafted amphiphilic polymer, hydrophobic pockets can form between the hydrophobic side chains of the polymers and the oleic acid on UCNPs' surface, thus enabling encapsulation of anticancer drug molecules (e.g., doxorubicin). The releasing of doxorubicin can be controlled by pH, with increased dissociation rate in acid conditions, which is favorable for drug releasing in tumor cells. The intracellular delivery process of doxorubicin can be monitored by a laser scanning confocal microscope. In another way, drugs can be deposited in the pores of mesoporous silica shell coated onto UCNPs. For example, ibuprofen was studied as a model drug and loaded onto mesoporous silica-coated -$NaYF_4$:Yb,Er UCNP fibers by electro-spinning process [48]. Large ibuprofen loading amount can be performed because of the high specific surface area and large pore volume of silica shell. After loading ibuprofen, significant upconverting luminescence quenching will occur; thus, the loading quantity can be determined by measuring the quenching extent,

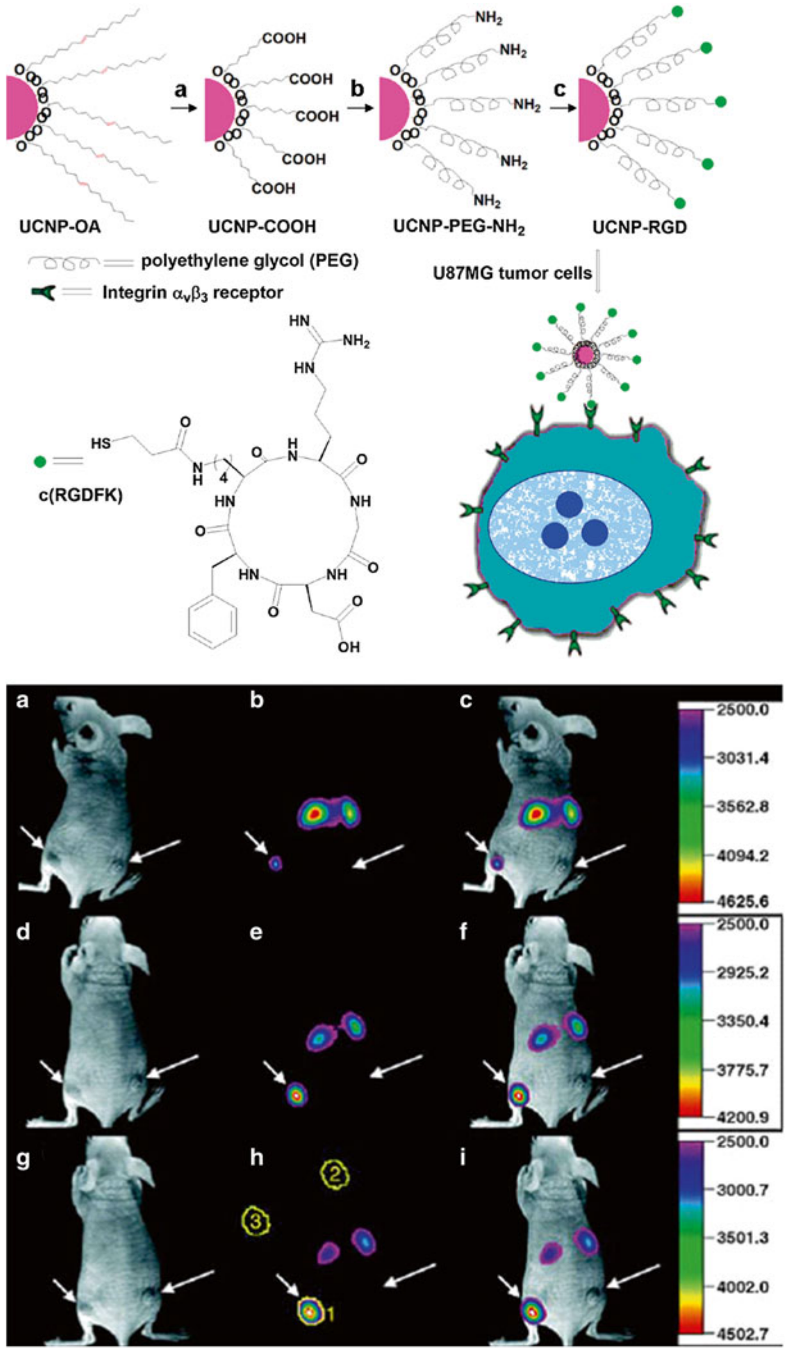

Fig. 4.11 Illustration scheme for UCNP-RGD and in vivo upconversion luminescence imaging of subcutaneous U87MG tumor (*left* hind leg) and MCF-7 tumor (*right* hind leg) after intravenous injection of UCNP-RGD conjugate over 24-h period (Reprinted with the permission from Ref. [38]. Copyright 2009 American Chemical Society)

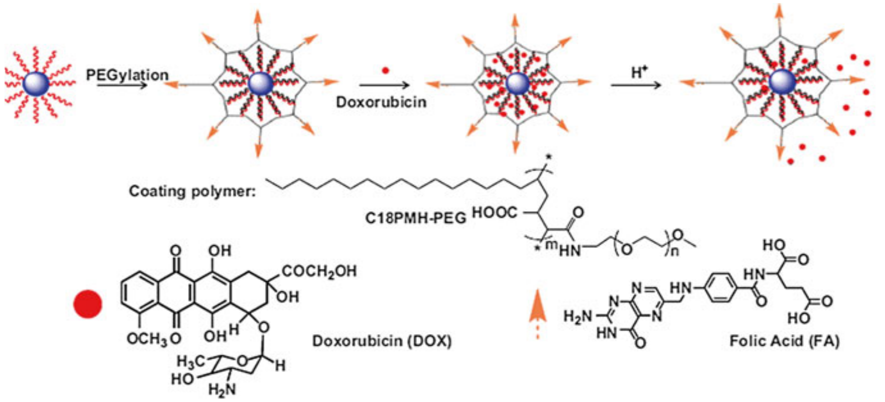

Fig. 4.12 Schematic illustration of the UCNP-based drug delivery system. (*a*) As-synthesized oleic acid capped UCNPs, (*b*) C18PMH-PEG-FA functionalized UCNPs, and (*c*) DOX loading on UCNPs. DOX molecules are physically adsorbed into the oleic acid layer on the nanoparticle surface by hydrophobic interactions. (*d*) Release of DOX from UCNPs triggered by decreasing pH (Reprinted from Ref. [47], Copyright 2011, with permission from Elsevier)

and more importantly, the subsequent drug releasing can be monitored by the recovering of luminescence intensity.

4.5.2 Light-Controllable Drug Release Based on UCNPs

Releasing bioactive molecules or drugs at desired time and location is of great interest for delivery systems development, in which way determinative therapeutic and diagnostic consequence can be greatly enhanced with minimized side effects during treatment. In addition, studies at directing cellular processes and disease regulation would benefit from the delivery of multi-payloads in varied doses at different time intervals [49, 50]. Among the release controlling methods, light-triggered molecular cleavage has received growing interest, due to the well-defined time and spatial drug releasing, thus offering unique precisely compared with other classical stimuli. Using the upconversion properties of UCNPs, remote control of photo-release of imaging probes and drug payloads has been demonstrated. For example, NIR light-responsive cross-linked mesoporous silica-coated UCNP drug delivery conjugate has been designed as photocaged nanocarriers (Fig. 4.13) [50]. The lanthanide-doped UCNPs were first coated with silica shell and followed by polymerization of 1-(2-nitrophenyl)ethyl photocaged oligo(ethylene) glycol vinyl monomers. Antitumor drug (doxorubicin) was able to be encapsulated in the hydrophobic pockets within the aforementioned polymer. Under NIR light irradiation, the cleavage of the cross-linked photocaged linker can be triggered by the upconverting emissions from UCNPs, and precisely release of targeted drug can be performed at controlled position and regulated time.

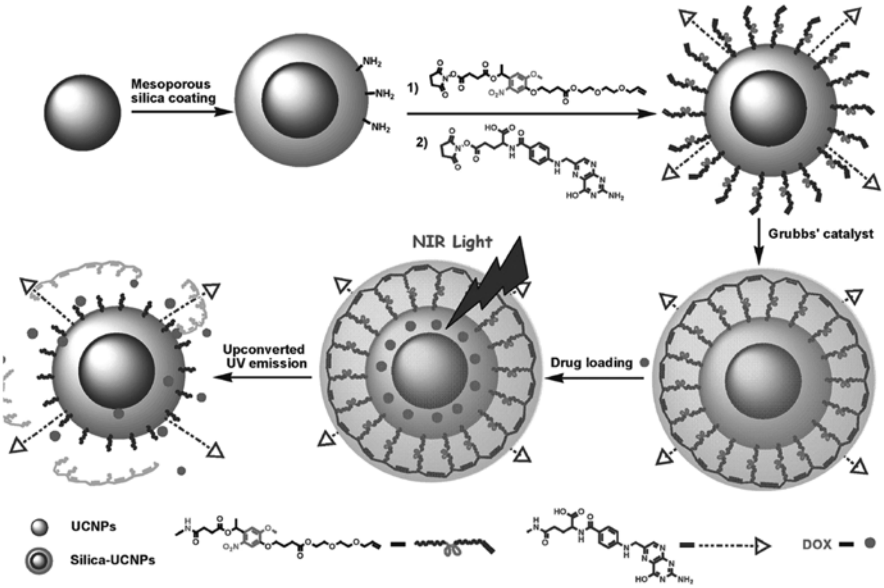

Fig. 4.13 Illustration for photocontrolled DOX delivery through photocage mesoporous silica-coated UCNPs (Reproduced from Ref. [50] by permission of John Wiley & Sons Ltd.)

4.5.3 UCNPs for Gene Delivery

The limitation for gene therapy is designing effective gene delivery vectors for specific and controllable delivering gene cargoes into living cells and tissues. There is a growing interest for developing nonviral synthetic nanocarriers for gene delivery [51]. Such carriers require four important factors, namely, (1) biocompatible, (2) traceable by long-term and real-time imaging, (3) controllable release, and (4) targeting. UCNPs have been employed to deliver nucleic acids in gene therapy and exhibit promising benefits. For example, silica-coated -$NaYF_4$:Yb, Er UCNPs were used to track the delivery of siRNA into cells using luminescence resonance energy transfer system for studying the intracellular uptake, release, and biostability of UCNP-bound siRNA in live cells [52]. In this system, cationic silica-coated -$NaYF_4$:Yb, Er acts as the donor and the siRNA-intercalating dye BOBO-3 as the corresponding acceptor. Under 980 nm excitation, the nanoparticles emit upconverted fluorescence at the wavelength of 543 nm, which was consequently absorbed by BOBO-3-stained siRNA (siRNA-BOBO3) acceptor via overlapped absorption band. These UCNPs were shown to bind and protect siRNA from RNase cleavage and to effectively deliver siRNA into cells. Under excitation at 980 nm, when the amino-modified UCNPs were bound with BOBO-3-stained siRNA, energy was allowed to transfer from UCNPs to BOBO-3 and consequently generate characteristic BOBO emissions at 602 nm (Fig. 4.14). Once the siRNA was separated from UCNPs, the energy transfer process was inhibited. The results showed that siRNA

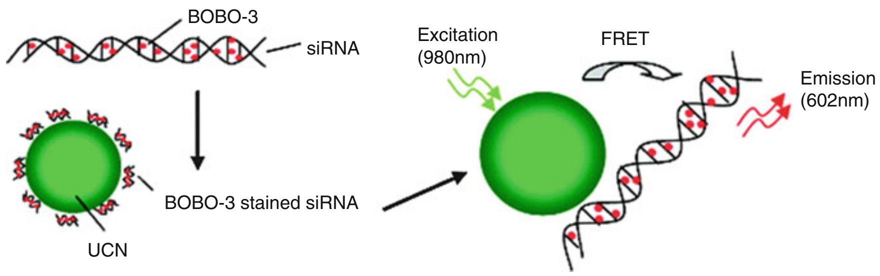

Fig. 4.14 Schematic drawing of FRET-based UCN/siRNA-BOBO3 complex system. siRNA is stained with BOBO-3 dyes, and the stained siRNA is attached to the surface of $NaYF_4$:Yb,Er nanoparticles. Upon excitation of the nanoparticles at 980 nm, energy is transferred from the donor (UCN) to the acceptor (BOBO-3) (Reprinted with the permission from Ref. [52]. Copyright 2010 American Chemical Society)

could gradually release from the UCNPs' surface into the cytoplasm over 24 h. Subsequently, similar strategy was used to monitor green fluorescent protein (GFP)-encoded plasmid DNA delivery and release in live cells [53].

4.6 UCNPs as Phototherapeutic Reagents

4.6.1 Photodynamic Therapy

Typical photosensitizer is capable of excitation under visible light and generates cytotoxic reactive oxygen species (ROS) which can be used to kill tumor cells. Only light, neither toxic nor invasive, is used as the therapeutic reagents in such process, namely, photodynamic therapy (PDT) [54]. Yet, such wavelength of light has rather limited tissue penetration depth (<1 cm). A promising nanocarrier and energy donor for these sensitizers is NIR-excitable UCNPs [55]. The design of UCNP-based PDT system includes the aforementioned UCNPs, surface coating, and the hereafter photosensitizers. Ideally, a photosensitizer should have good ROS production efficiency, a high absorption coefficient at longer wavelengths for better tissue penetration, amphiphilicity, low dark toxicity, ease of synthesis, and ease of formulation in aqueous solvents for in vivo delivery. Several different kinds of photosensitizers have been developed for PDT, and they can be broadly classified into chemical groups such as porphyrins, phthalocyanines, chlorins, 5-aminolevulinic acid (ALA), and naphthalocyanines; photosensitizers like porfimer sodium, temoporfin, 5-aminolevulinic acid, methyl aminolevulinate, hexyl aminolevulinate, talaporfin sodium, aluminum phthalocyanine disulfonate, tin ethyl etiopurpurin, and verteporfin have been approved for clinical use [8].

For example, tris(bipyridine)ruthenium(II) ($Ru(bpy)_3^{2+}$)-doped SiO_2 shell was used to encapsulate $NaYF_4$:Yb,Tm core [56]. Under 980 nm excitation, the blue emission from Tm^{3+} could be absorbed by $^1O_2$ generator $Ru(bpy)_3^{2+}$, and the consequently generated $^1O_2$ could be detected by chemical method. For the purpose of increase loading amount of photosensitizer, $NaYF_4$:Yb,Er nanoparticles were fabricated with 100 nm size, and 10 wt.% photosensitizer loading ratio was achieved by coating meso-tetraphenylporphine in poly(ethylene glycol-block-(DL)lactic acid) [57]. Using this system, efficient cancer cell killing activity was observed on NIR excitation, with low cytotoxicity in the absence of NIR light. Moreover, in vivo UCNP-based PDT system was introduced by non-covalently incorporating photosensitizing porphyrin derivative into amphiphilic polymer-coated $NaYF_4$:Yb,Er nanoparticles. Excellent tumor regression was observed under 980 nm CW laser excitation, plus low toxicity and gradual clearout from mouse organs (Fig. 4.15) [58].

Recently, we developed high Yb-doped UCNPs with a biocompatible CaF_2 shell with an optimal 15-fold increase in red emissions compared to their hexagonal phased counterparts. The absolute quantum yield of R-NaYF4:80 %Yb,2 %Er@

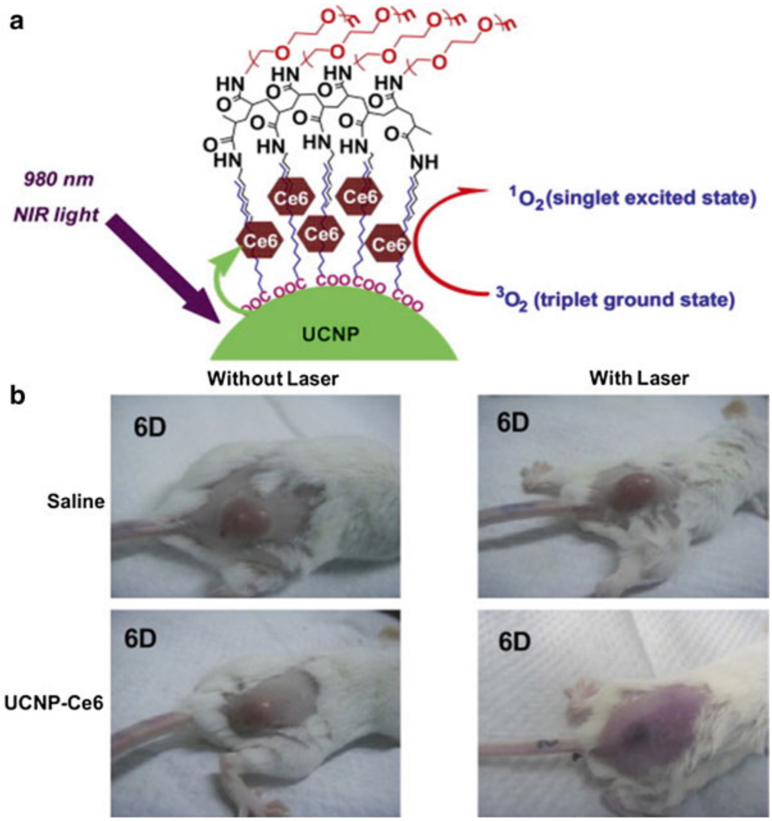

Fig. 4.15 (**a**) A schematic drawing showing NIR-induced PDT using UCNP-Ce6. (**b**) Representative photos of mice after various treatments indicated at the sixth day (Reprinted from ref. [58], Copyright 2011, with permission from Elsevier)

CaF2 is measured to be 3.2 ± 0.1 %, the highest reported value for red emissions. Furthermore, we demonstrate conjugating ALA (aminolevulinic acid), a clinically used prodrug for the red absorbing photosensitizer PpIX, to the UCNP surface via a hydrazone linkage, giving us exquisite control over their PDT effect in the cell. This photodynamic therapy system was tested for its therapeutic potential: it exhibited strong singlet oxygen generation and ~70 % cell death after 20 min of NIR irradiation. Furthermore, significant cell death (~30 %) was produced in simulated deep tumor conditions with as much as 12 mm of pork tissue and a biocompatible low power density of 0.5 W/cm^2, while ALA-UCNPs based on the known optimal red-emitting UCNP cannot. Finally, in vivo mice models of tumors when treated with these ALA-UCNPs demonstrated size reduction significant from the controls even under 12 mm of pork tissue (the greatest depth at which UCNP PDT has been achieved), while clinically used red light could not (Fig. 4.16) [59]. This study marks an important step forward in biocompatible photodynamic therapy utilizing UCNPs to effectively access deep-set tumors at a low irradiation power density. It may also provide new opportunities for a variety of applications using upconverting red radiation in photonics and biophotonics.

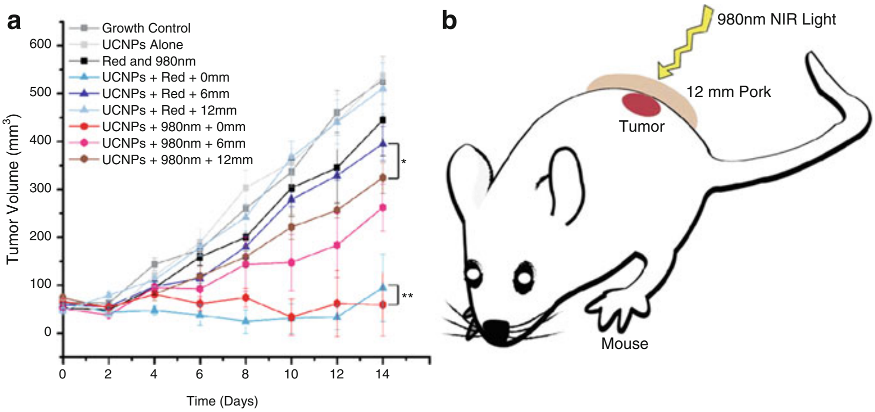

Fig. 4.16 In vivo volume of tumors exposed to various controls and ALA-UCNPs with red and near-infrared irradiation (0.5 w/cm^2) in simulated deep tumors. Growth control, untreated tumors; UCNPs alone, tumors exposed to ALA-UCNPs without irradiation; red and 980 nm, tumors simultaneously exposed to red and NIR light both at 0.5 w/cm^2 but no ALA-UCNPs; UCNPs+red+0 mm, tumors exposed to ALA-UCNPs and clinically used red light; UCNPs+red+6 mm, tumors 6 mm deep exposed to ALA-UCNPs and clinically used red light; UCNPs+red+12 mm, tumors 12 mm deep exposed to ALA-UCNPs and clinically red light; UCNPs+980 nm+0 mm, tumors exposed to ALA-UCNPs and NIR light; UCNPs+980 nm+ 6 mm, tumors 6 mm deep exposed to ALA-UCNPs and NIR light; UCNPs+980 nm+12 mm, tumors 12 mm deep exposed to ALA-UCNPs and NIR light. Statistical significance was determined from one-way t-tests; significance (8) was based on $p < 0.05$ and $P > 0.05$ for not significant (**) pairs (Reprinted with the permission from Ref. [59]. Copyright 2014 American Chemical Society)

4.6.2 Photothermal Therapy

The basic model for photothermal therapy (PTT) is in part similar with PDT, in which vibrational energy (heat) is generated from photosensitizer for cell killings [60]. -$NaYF_4$:Yb,Er nanoparticles were coated with silver shell with stronger plasmonic resonance performance, and PTT was applied in vitro on HepG2 and BCap-37 cells from human hepatic cancer and human breast cancer separately [61].

In order to achieve a multimodal cancer therapy, multifunctional core/satellite nanotheranostic was developed by attaching ultrasmall CuS nanoparticles onto the surface of silica-coated UCNPs (Fig. 4.17). These nanocomposites exhibit many advantages as multifunctional nanotheranostics, such as (1) NIR light can be transferred to local thermal energy for photothermal therapy agents; (2) Z elements (Yb, Gd, and Er) can cause large local radiation dose enhancement around nanoparticles as radiosensitizers; and (3) UCL/MR/CT trimodal imaging could be simultaneously performed with this multifunctional nanotheranostic. This development laid the groundwork for the image-guided therapy in the future [62].

4.6.3 Combined PDT/PTT

A surface functionalization strategy was developed for UCNPs by coating those nanoparticles with BSA protein [63]. In such a UCNP@BSA system, the Gd-based UCNPs, which are useful contrast agents for dual modal optical/MR imaging, in the mean time are able to trigger photodynamic therapy under NIR light by resonance energy transfer if coupled with photosensitizers. On the other hand, the BSA coating not only improves the physiological stability of UCNPs but also could serve as a delivery platform to load various molecules with therapeutic functions. RB, a photodynamic agent, together with IR825, a photothermal agent, is simultaneously

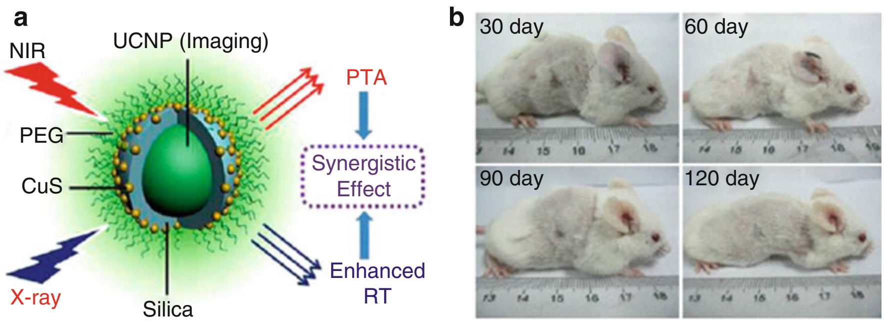

Fig. 4.17 (**a**) Illustration of nanocarriers for enhanced photothermal ablation and radiotherapy synergistic therapy; (**b**) photographs of mice in 30, 60, 90, and 120 days of treatment, showing complete eradication of the tumor and no visible recurrences of the tumors in at least 120 days (Reprinted with the permission from Ref. [62]. Copyright 2013 American Chemical Society)

loaded on UCNP@BSA for combined phototherapy of cancer, demonstrating outstanding synergistic antitumor effect in our animal experiments. Although further studies are still ongoing in our laboratory aiming at achieving combination therapy of cancer upon systemic administration (e.g., intravenous injection) of such UCNP-based theranostic agent, our work presents a new design of a simple nanoplatform, in which multiple imaging and therapy functions can be integrated together for imaging-guided cancer combination therapy (Fig. 4.18).

4.7 Conclusion and Prospects

In the past decade, we have witnessed the rapid development of UCNPs both in synthesis and applications. The unique optical properties and outperformed chemical and physical behaviors of UCNPs make them attractive candidates for bio-related applications, especially bio-imaging, drug delivery, and photodynamic therapy. Their UV/vis emission can be excited by biotissue-penetrable NIR light, which endows them deep tissue applications such as remote switchable smart bio-devices and NIR-driven PDT process. However, the upconversion efficiency of lanthanide-based UCNPs is still very low, especially under low power density excitation. Moreover, it is still challenging to generate small UCNPs, especially sub-10 nm, without sacrificing the upconversion efficiency. In addition, the development of commercially available systems of more versatile UCNPs with unique excitation and emission wavelength is critical to expand the applications of UCNPs. Meanwhile, further work is needed for better understanding the uptake, release rate, and toxicity of UCNPs for harnessing these nanoplatforms for applications in photonics and biophotonics.

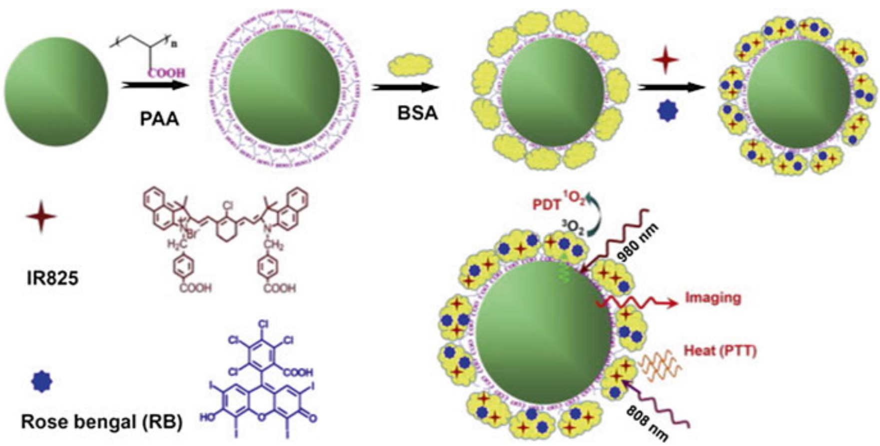

Fig. 4.18 A schematic illustration to show the synthesis of UCNP@BSA-RB&IR825 nanocomplex and the mechanism of both PDT and PTT therapies based on this system (Reprinted from Ref. [63], Copyright 2014, with permission from Elsevier)

References

1. Auzel F (2004) Upconversion and anti-stokes processes with f and d ions in solids. Chem Rev 104(1):139–173
2. Wu X, Chen G, Shen J et al (2015) Upconversion nanoparticles: a versatile solution to multi-scale biological imaging. Bioconjug Chem 28(2):166–175
3. Wu SW, Han G, Milliron DJ et al (2009) Non-blinking and photostable upconverted luminescence from single lanthanide-doped nanocrystals. Proc Natl Acad Sci U S A 106(27):10917–10921
4. Liu Q, Feng W, Yang TS et al (2013) Upconversion luminescence imaging of cells and small animals. Nat Protoc 8(10):2033–2044
5. Chen GY, Shen J, Ohulchanskyy TY et al (2012) (α-$NaYbF_4$:Tm^{3+})/CaF_2 core/shell nanoparticles with efficient near-infrared to near-infrared upconversion for high-contrast deep tissue bioimaging. ACS Nano 6(9):8280–8287
6. Yang TS, Liu Q, Li JC et al (2014) Photoswitchable upconversion nanophosphors for small animal imaging in vivo. R Soc Chem Adv 4(30):15613–15619
7. Shen J, Zhao L, Han G (2013) Lanthanide-doped upconverting luminescent nanoparticle platforms for optical imaging-guided drug delivery and therapy. Adv Drug Deliv Rev 65(5):744–755
8. Idris NM, Jayakumar MKG, Bansal A et al (2015) Upconversion nanoparticles as versatile light nanotransducers for photoactivation applications. Chem Soc Rev 44(6):1449–1478
9. Wang J, Deng RR, MacDonald MA et al (2014) Enhancing multiphoton upconversion through energy clustering at sublattice level. Nat Mater 13(2):157–162
10. Liu Q, Sun Y, Yang TS et al (2011) Sub-10 nm hexagonal lanthanide-doped NaLuF4 upconversion nanocrystals for sensitive bioimaging in vivo. J Am Chem Soc 133(43):17122–17125
11. Ryu J, Park HY, Kim K et al (2010) Facile synthesis of ultrasmall and hexagonal NaGdF4: Yb3+, Er3+ nanoparticles with magnetic and upconversion imaging properties. J Phys Chem C 114(49):21077–21082
12. Shen J, Chen GY, Vu AM et al (2013) Engineering the upconversion nanoparticle excitation wavelength: cascade sensitization of tri-doped upconversion colloidal nanoparticles at 800 nm. Adv Opt Mater 1(9):644–650
13. Qiu PY, Zhou N, Chen HY et al (2013) Recent advances in lanthanide-doped upconversion nanomaterials: synthesis, nanostructures and surface modification. Nanoscale 5(23):11512–11525
14. Mai HX, Zhang YW, Si R et al (2006) High-quality sodium rare-earth fluoride nanocrystals: controlled synthesis and optical properties. J Am Chem Soc 128(19):6426–6436
15. Yi GS, Chow GM (2006) Synthesis of hexagonal-phase NaYF4: Yb, Er and NaYF4: Yb, Tm nanocrystals with efficient up-conversion fluorescence. Adv Funct Mater 16(18):2324–2329
16. Boyer JC, Vetrone F, Cuccia LA et al (2006) Synthesis of colloidal upconverting NaYF4 nanocrystals doped with Er^{3+}, Yb^{3+} and Tm^{3+}, Yb^{3+} via thermal decomposition of lanthanide trifluoroacetate precursors. J Am Chem Soc 128(23):7444–7445
17. Boyer JC, Cuccia LA, Capobianco JA (2007) Synthesis of colloidal upconverting NaYF4: Er3+/Yb3+ and Tm3+/Yb3+ monodisperse nanocrystals. Nano Lett 7(3):847–852
18. Yi GS, Chow GM (2007) Water-soluble NaYF4: Yb, Er(Tm)/NaYF4/polymer core/shell/shell nanoparticles with significant enhancement of upconversion fluorescence. Chem Mater 19(3):341–343
19. Zeng JH, Su J, Li ZH et al (2005) Synthesis and upconversion luminescence of hexagonal-phase NaYF4: Yb, Er, phosphors of controlled size and morphology. Adv Mater 17(17):2119–2123
20. Wang X, Zhuang J, Peng Q et al (2005) A general strategy for nanocrystal synthesis. Nature 437(7055):121–124
21. Liang X, Wang X, Zhuang J et al (2007) Synthesis of NaYF4 nanocrystals with predictable phase and shape. Adv Funct Mater 17(15):2757–2765

22. Wang Y, Tu LP, Zhao JW et al (2009) Upconversion luminescence of beta-NaYF4: Yb^{3+}, Er^{3+}@β-$NaYF_4$ core/shell nanoparticles: excitation power, density and surface dependence. J Phys Chem C 113(17):7164–7169
23. Wang F, Wang JA, Liu XG (2010) Direct evidence of a surface quenching effect on size-dependent luminescence of upconversion nanoparticles. Angew Chem Int Ed 49(41):7456–7460
24. Shen J, Chen GY, Ohulchanskyy TY et al (2013) Tunable near infrared to ultraviolet upconversion luminescence enhancement in (α-NaYF4:Yb, Tm)/CaF2 core/shell nanoparticles for in situ real-time recorded biocompatible photoactivation. Small 9(19):3213–3217
25. Zhong YT, Tian G, Gu ZJ et al (2014) Elimination of photon quenching by a transition layer to fabricate a quenching-shield sandwich structure for 800 nm excited upconversion luminescence of Nd^{3+} sensitized nanoparticles. Adv Mater 26(18):2831–2837
26. Wen HL, Zhu H, Chen X et al (2013) Upconverting near-infrared light through energy management in core-shell-shell nanoparticles. Angew Chem Int Ed 52(50):13419–13423
27. Lai J, Zhang Y, Pasquale N et al (2014) An upconversion nanoparticle with orthogonal emissions using dual NIR excitations for controlled two-way photoswitching. Angew Chem Int Ed 126(52):14647–14651
28. Zhao L, Kutikov A, Shen J et al (2013) Stem cell labeling using polyethylenimine conjugated (α-$NaYbF_4$:Tm^{3+})/CaF_2 upconversion nanoparticles. Theranostics 3(4):249–257
29. Chen ZG, Chen HL, Hu H et al (2008) Versatile synthesis strategy for carboxylic acid-functionalized upconverting nanophosphors as biological labels. J Am Chem Soc 130(10):3023–3029
30. Zhang TR, Ge JP, Hu YX et al (2007) A general approach for transferring hydrophobic nanocrystals into water. Nano Lett 7(10):3203–3207
31. Dong AG, Ye XC, Chen J et al (2011) A generalized ligand-exchange strategy enabling sequential surface functionalization of colloidal nanocrystals. J Am Chem Soc 133(4):998–1006
32. Conner SD, Schmid SL (2003) Regulated portals of entry into the cell. Nature 422(6927):37–44
33. Jin JF, Gu YJ, Man CWY et al (2011) Polymer-coated $NaYF_4$:Yb^{3+}, Er^{3+} upconversion nanoparticles for charge-dependent cellular imaging. ACS Nano 5(10):7838–7847
34. Cao TY, Yang Y, Gao YA et al (2011) High-quality water-soluble and surface-functionalized upconversion nanocrystals as luminescent probes for bioimaging. Biomaterials 32(11):2959–2968
35. Zhou J, Zhu XJ, Chen M et al (2012) Water-stable NaLuF4-based upconversion nanophosphors with long-term validity for multimodal lymphatic imaging. Biomaterials 33(26):6201–6210
36. Peng JJ, Sun Y, Zhao LZ et al (2013) Polyphosphoric acid capping radioactive/upconverting NaLuF4:Yb, Tm, Sm-153 nanoparticles for blood pool imaging in vivo. Biomaterials 34(37):9535–9544
37. Xiong LQ, Chen ZG, Yu MX et al (2009) Synthesis, characterization, and in vivo targeted imaging of amine-functionalized rare-earth up-converting nanophosphors. Biomaterials 30(29):5592–5600
38. Xiong LQ, Chen ZG, Tian QW et al (2009) High contrast upconversion luminescence targeted imaging in vivo using peptide-labeled nanophosphors. Anal Chem 81(21):8687–8694
39. Yu XF, Sun ZB, Li M et al (2010) Neurotoxin-conjugated upconversion nanoprobes for direct visualization of tumors under near-infrared irradiation. Biomaterials 31(33):8724–8731
40. Bogdan N, Rodriguez EM, Sanz-Rodriguez F et al (2012) Bio-functionalization of ligand-free upconverting lanthanide doped nanoparticles for bio-imaging and cell targeting. Nanoscale 4(12):3647–3650
41. Wang M, Mi CC, Wang WX et al (2009) Immunolabeling and NIR-excited fluorescent imaging of HeLa cells by using NaYF4:Yb, Er upconversion nanoparticles. ACS Nano 3(6):1580–1586

42. Xiong LQ, Yang TS, Yang Y et al (2010) Long-term in vivo biodistribution imaging and toxicity of polyacrylic acid-coated upconversion nanophosphors. Biomaterials 31(27):7078–7085
43. Cheng L, Yang K, Shao MW et al (2011) In vivo pharmacokinetics, long-term biodistribution and toxicology study of functionalized upconversion nanoparticles in mice. Nanomedicine 6(8):1327–1340
44. Bridot JL, Faure AC, Laurent S et al (2007) Hybrid gadolinium oxide nanoparticles: multimodal contrast agents for in vivo imaging. J Am Chem Soc 129(16):5076–5084
45. Liu CY, Gao ZY, Zeng JF et al (2013) Magnetic/upconversion fluorescent NaGdF4:Yb, Er nanoparticle-based dual-modal molecular probes for imaging tiny tumors in vivo. ACS Nano 7(8):7227–7240
46. Jalil RA, Zhang Y (2008) Biocompatibility of silica coated NaYF4 upconversion fluorescent nanocrystals. Biomaterials 29(30):4122–4128
47. Wang C, Cheng LA, Liu ZA (2011) Drug delivery with upconversion nanoparticles for multifunctional targeted cancer cell imaging and therapy. Biomaterials 32(4):1110–1120
48. Hou ZY, Li CX, Ma PA et al (2011) Electrospinning preparation and drug-delivery properties of an up-conversion luminescent porous $NaYF_4$:Yb^{3+}, Er^{3+}@silica fiber nanocomposite. Adv Funct Mater 21(12):2356–2365
49. Min YZ, Li JM, Liu F et al (2014) Near-infrared light-mediated photoactivation of a platinum antitumor prodrug and simultaneous cellular apoptosis imaging by upconversion-luminescent nanoparticles. Angew Chem Int Ed 53(4):1012–1016
50. Yang YM, Velmurugan B, Liu XG et al (2013) NIR photoresponsive crosslinked upconverting nanocarriers toward selective intracellular drug release. Small 9(17):2937–2944
51. Thomas M, Klibanov AM (2003) Non-viral gene therapy: polycation-mediated DNA delivery. Appl Microbiol Biotechnol 62(1):27–34
52. Jiang S, Zhang Y (2010) Upconversion nanoparticle-based FRET system for study of siRNA in live cells. Langmuir 26(9):6689–6694
53. Guo HC, Idris NM, Zhang Y (2011) LRET-based biodetection of DNA release in live cells using surface-modified upconverting fluorescent nanoparticles. Langmuir 27(6):2854–2860
54. Fisher AMR, Murphree AL, Gomer CJ (1995) Clinical and preclinical photodynamic therapy. Laser Surg Med 17(1):2–31
55. Shan GB, Weissleder R, Hilderbrand SA (2013) Upconverting organic dye doped core-shell nano-composites for dual-modality NIR imaging and photo-thermal therapy. Theranostics 3(4):267–274
56. Guo YY, Kumar M, Zhang P (2007) Nanoparticle-based photosensitizers under CW infrared excitation. Chem Mater 19(25):6071–6072
57. Shan JN, Budijono SJ, Hu GH et al (2011) Pegylated composite nanoparticles containing upconverting phosphors and meso-tetraphenyl porphine (TPP) for photodynamic therapy. Adv Funct Mater 21(13):2488–2495
58. Wang C, Tao HQ, Cheng L et al (2011) Near-infrared light induced in vivo photodynamic therapy of cancer based on upconversion nanoparticles. Biomaterials 32(26):6145–6154
59. Punjabi A, Wu X, Tokatli-Apollon A et al (2014) Amplifying the red-emission of upconverting nanoparticles for biocompatible clinically used prodrug-induced photodynamic therapy. ACS Nano 8(10):10621–10630
60. Saxton RE, Paiva MB, Lufkin RB, Castro DJ (1995) Laser photochemotherapy – a less invasive approach for treatment of cancer. Semin Surg Oncol 11(4):283–289
61. Dong BA, Xu S, Sun JA et al (2011) Multifunctional $NaYF_4$: Yb^{3+}, Er^{3+}@Agcore/shell nanocomposites: integration of upconversion imaging and photothermal therapy. J Mater Chem 21(17):6193–6200
62. Xiao QF, Zheng XP, Bu WB et al (2013) A core/satellite multifunctional nanotheranostic for in vivo imaging and tumor eradication by radiation/photothermal synergistic therapy. J Am Chem Soc 135(35):13041–13048
63. Chen Q, Wang C, Cheng L et al (2014) Protein modified upconversion nanoparticles for imaging-guided combined photothermal and photodynamic therapy. Biomaterials 35(9):2915–2923